Vibrational structure of d-excitons in layered manganese dihalides

1984 J. Phys. C: Solid State Phys. 17 4519

(http://iopscience.iop.org/0022-3719/17/25/014)

J. Phys. C: Solid State Phys., 17 (1984) 4519–4527. Printed in Great Britain

Vibrational structure of d-excitons in layered manganese dihalides

L Piseri† and I Pollini‡

† Istituto di Chimica delle Macromolecole del CNR, Via E Bassini 15/A, 20133 Milano, Italy

‡ Dipartimento di Fisica, Università di Milano and Gruppo Nazionale di Struttura della Materia del CNR, Via Celoria 16, 20133 Milano, Italy

Received 6 February 1984

Abstract. The complex multiphonon fine structure of the d–d absorption bands $^4E_g(D)$, $^4E_g(G)$ and $^4A_{1g}(G)$ in manganese dihalides is studied in detail by a fitting procedure. With this aim, an analytical expression for the absorption coefficient has been deduced, from the Fourier transform of the optical response function for weak electron–phonon interaction in the adiabatic and Condon approximations. The observed vibrational structure of these crystals is in general well accounted for by the superposition of one-phonon progressions, except for the intraconfigurational $^6A_{1g} \rightarrow {}^4E_g(D)$ band of $MnCl_2$ where the contribution of a two-phonon progression of E_g symmetry is essential to reproduce the shape of the optical profile. The long-wavelength phonon frequencies on Mn halides and Fe, Co and Ni iodides have also been measured by far-infrared transmission and Raman scattering techniques.

1. Introduction

Transition-metal halides (TMH) exhibit complex absorption structures occurring in the near-infrared and visible regions of the spectrum. The absorption bands have been attributed to electric dipole forbidden transitions, activated by electron–phonon (e–p) interaction, between the transition-metal d-levels as split by the crystal field of the surrounding halogens (McClure 1959). The primary and most evident effect of the electron–phonon coupling is represented by the multiphonon fine structure forming the various progressions observed in absorption or emission spectra. Their assignment to phonon sidebands, rather than to dynamical Jahn–Teller-induced vibronic features, is mainly based on the fact that the spacing of the repetitive patterns corresponds to the A_{1g} and/or E_g Raman-active modes of the lattice. Depending on the strength of the e–p interaction, which affects the lineshape of the absorption curve, the number of phonons involved may vary greatly in number from the case in which there is no interaction at all (zero-phonon lines for parity-allowed transitions) to the case of strong interaction with many phonons involved (Chiarotti 1971).

Inelastic neutron scattering measurements in $MnCl_2$ (Escribe *et al* 1980) and $FeBr_2$ (Yelon *et al* 1980) and lattice dynamical calculations on a series of TMH crystals (Benedek and Frey 1980) have shown that the dispersion curves associated with the Raman-active modes are quite flat producing sharply peaked density of states. This allows for the

0022-3719/84/254419 + 09 $02.25

experimental observation of sharp phonon progressions in the absorption spectra of $d^n \rightarrow d^n$ parity-forbidden transitions for this class of crystals (Pollini *et al* 1980).

An interesting case, frequently occurring in TMH, is that of isoconfigurational (IC) transitions for which both first- and second-order progressions are possible, as it has been shown in the case of $NiCl_2$ and $NiBr_2$ (Benedek *et al* 1979). As a matter of fact, for IC transitions in half-filled shells ($d^3(t_{2g}^3)$, $d^5(t_{2g}^3, e_g^2)$, $d^8(e_g^2)$) the orbital e–p coupling vanishes to first order (Sugano *et al* 1970): thus a second-order progression is expected to be the basic vibronic structure, provided that also the spin-dependent e–p interaction is zero. Such a selection rule is also fulfilled by the transitions $^6A_{1g}(S) \rightarrow {}^4E_g(G) + {}^4A_{1g}(G)$ and $^6A_{1g}(S) \rightarrow {}^4E_g(D)$ for the d^5 electronic configuration in Mn halides for which the interpretation in terms of phonon progressions is still controversial.

For these reasons, we have re-examined these crystal-field transitions of MnX_2 (X = Cl, Br, I) and measured their Raman and far-infrared (FIR) spectra. The analysis of the absorption spectrum has been then made by a least-squares fitting procedure. With this aim, on the basis of few approximations, we have been able to derive an analytical expression for the absorption coefficient.

2. Experimental

The manganese dihalides MnX_2 crystallise in a layered structure either of the $CdCl_2$ type (C19), as $MnCl_2$, or the CdI_2 type (C6), as $MnBr_2$ and MnI_2. Their respective symmetry classes are D_{3d}^5 or D_{3d}^3, and the metal ions are centres of D_{3d} symmetry in both structures. The nearest neighbours of the metal atom form a slightly distorted octahedron. Furthermore, NiI_2 crystallises in the $CdCl_2$-type structure, and FeI_2 and CoI_2 in the CdI_2-type (Wyckoff 1972). In both crystal structures the primitive crystallographic cell contains one formula unit, and a factor group analysis yields four fundamental optic modes at the Γ point: $A_{1g} + E_g + A_{2u} + E_u$, i.e. two Raman-active (even) modes and two infrared-active (odd) modes. If we look at the eigenvectors of the zone-centre optical modes of the previous structures we find that the atoms vibrate within the layers in the E modes and perpendicular to the layers in the A modes.

Single crystals of $MnCl_2$ and $MnBr_2$ have been grown from the vapour phase by means of a flow system using pure elements as starting materials (Mn, 99.99%; Merck). Typical growth temperatures were around 550 °C for $MnCl_2$ and 500 °C for $MnBr_2$. The crystals of MI_2 (M = Mn, Co, Fe) have been obtained by heating stoichiometric amounts of transition-metal powders and very pure iodine in a sealed quartz tube with a temperature gradient of approximately 200–550 °C. Microcrystalline powders of NiI_2 have been instead obtained by direct reaction of stoichiometric quantities of the elements in ethanol solution at room temperature. All crystals are quite hygroscopic so that their transfer into the cryostat used for the spectroscopic measurements had to be made with exclusion of air and moisture. In particular, for FIR measurements, microcrystalline flakes from the reaction ampoule were used and pellets were then pressed from a mixture of powdered polyethylene and crystal flakes ground in a powder mill in dry atmosphere. FIR absorption spectra of MnX_2 and FeI_2, CoI_2 and NiI_2, here reported for completeness, (see figure 1(*b*) and (*c*)) were recorded at liquid nitrogen temperature in the range 50–350 cm^{-1} with a Hitachi Perkin–Elmer Mo FIS 3 spectrophotometer. The low-temperature infrared absorbance spectra were in general slightly better resolved, showing very small shifts in position to higher wavenumbers (in general, less than 5 cm^{-1}). The Raman scattering of MnX_2 (X = Cl, Br, I) (figure 1(*a*)) was excited with the 514.5

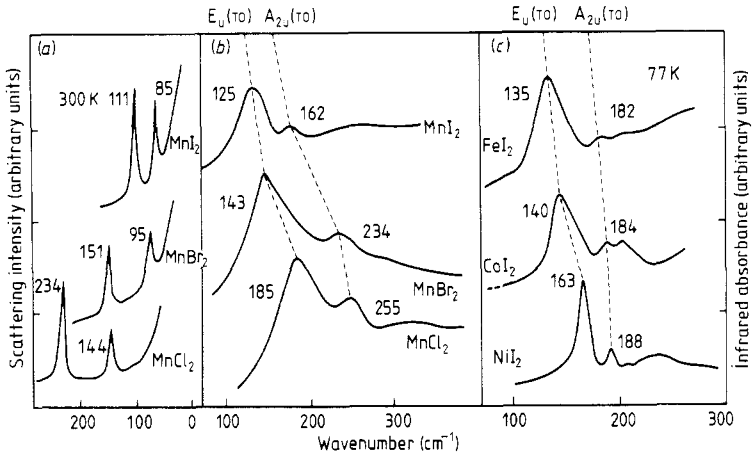

Figure 1. (*a*) Raman spectra of $MnCl_2$, $MnBr_2$ and MnI_2 single crystals at room temperature; (*b*) and (*c*) infrared absorption spectra of powdered Mn halides and Fe, Co and Ni diiodides imbedded in polyethylene. FIR measurements were taken at 300 K for $MnCl_2$ and $MnBr_2$ and at 77 K for the other pellets.

and 488 nm lines from an Ar/Kr laser of the Coherent Radiation (Mo 52MG). The laser light was directed along the *c* axis of the crystals and the scattered light at approximately 90° with respect to the incident beam was analysed by the double monochromator of a Jarrel–Ash 25–300 spectrophotometer and collected with a photomultiplier ITT EW-130. Table 1 gives the values of the infrared- and Raman-active modes measured in this work and listed together with the vibrational frequencies reported by other workers.

3. Theory

The electronic excitations which take place in TMH can be classified, on the basis of the exciton polaron model (Sumi 1974, 1975), as vibronic excitons with small excitation

Table 1. Vibrational frequency (cm^{-1}) of manganese halides and transition-metal iodides. Their assignments to optical active modes of the D_{3d} group are also indicated.

ω	$MnCl_2$	$MnBr_2$	MnI_2	FeI_2	CoI_2	NiI_2
A_{2u}(TO)	255	234	162	185	184	188
	287(LO)[a]				185[b]	178[c]
					191(LO)[c]	184(LO)[c]
Eu(TO)	185	143	125	135	140	163
	184[a]				152[b]	156[c]
					175(LO)[c]	176(TO)[c]
A_{1g}	234	151	112			
	242[b]					
E_g	144	90	85			
	150[b]					

[a] Campbell and Vickers (1983).
[b] Christie (1973).
[c] Kuindersma (1981).

transfer. The observed phonon progressions are in fact reminiscent of those predicted theoretically for small Huang–Rhys factor S_0 ($S_0 < 3$) and small exciton bandwidth ($B < 1$). The situation is very similar to that occurring for localised centres in semiconductors and insulators. The only difference is that these complex elementary excitations may interact with phonons via different mechanisms due to the two exciton degrees of freedom. In fact the photons can interact with excitons either through the centre-of-mass translation or through the hole–electron internal motion. Depending on which interaction is dominant one can have either phonon-assisted processes (semiconductors) or trapped excitons (alkali halides) which interact with phonons in the same way as in local centres (Knox 1973). The pronounced molecular character of TMH thus allows us to extend to this class of crystals the theoretical treatment generally used for localised electrons in insulating crystals and to derive the absorption coefficient within the framework of the interaction representation of the e–p operator (Perlin 1964).

By assuming adiabatic and Condon approximations, the absorption coefficient as a function of the frequency is given by:

$$\alpha(\Omega) = \frac{4\pi^2\Omega}{3hc\eta(\Omega)} I(\Omega) \tag{1}$$

with

$$I(\Omega) = \mathrm{Av}(n) \sum_{n'} |\langle fn'|M|in\rangle|^2 \delta\left(\Omega - \frac{E_{fn'} - E_{in}}{\hbar}\right), \tag{2}$$

where $\eta(\Omega)$ is the refractive index of the absorption medium, $\mathrm{Av}(n)$ indicates the thermal average over the ground-state vibronic levels $|in\rangle$, M is the electric dipole operator and $E_{fn'}$, E_{in} are the energies of the final and initial vibronic states respectively. In crystals possessing an inversion symmetry the electric dipole transitions between states of the same parity are assisted by odd-parity phonons and thus the electronic transition moment between states i and f is modified by the electron–phonon interaction $H_{\text{e-p}}$ as follows:

$$M_{\text{odd}} = \sum_j \left(\frac{\langle i|M|j\rangle\langle j|H_{\text{e-p}}|f\rangle}{E_j - E_f} + \frac{\langle f|M|j\rangle\langle j|H_{\text{e-p}}|i\rangle}{E_j - E_i}\right). \tag{3}$$

In this case the transition probability becomes

$$I(\Omega) = \mathrm{Av} \sum_{\substack{n' \\ (\text{even})}} |\langle n'|M_{\text{odd}}|n\rangle|^2 \delta\left(\Omega - \frac{E_{fn'} - E_{in}}{\hbar}\right). \tag{4}$$

where the thermal average is now performed only on *even phonon* states. By introducing the integral representation of the δ function and recalling that M_{odd} depends only upon odd-symmetry phonons, the Fourier transform of $I(\Omega)$ is then given by:

$$I(t) = |M_{\text{odd}}|^2 \mathrm{Av}(n)\langle n|\exp(-\mathrm{i}H_f t/\hbar)\exp(\mathrm{i}H_i t/\hbar)|n\rangle, \tag{5}$$

where H_i and H_f are the initial- and final-state Hamiltonians. In the 'displaced harmonic potential model' they can be written as:

$$H_i = \hbar\omega(b^+b + \tfrac{1}{2}) \tag{6}$$

$$H_f = H_i + \hbar\Omega_{if} + \hbar V^2/\omega - \hbar V(b + b^-) \tag{7}$$

where ω is the phonon frequency, b and b^+ are the boson operators, Ω_{if} is the frequency of the pure electronic transition, $\Omega_{if} + V^2/\omega$ is the vertical Frank–Condon frequency and V is the electron–vibrational coupling constant. By using the Feynman technique to disentangle the exponential operator factor, one gets:

$$I(t) = |M_{\mathrm{odd}}|^2 \exp(-\mathrm{i}\Omega_{if}t) \exp[-S(T)] \exp\{S_0[(\bar{n}+1)\,\mathrm{e}^{-\mathrm{i}\omega t} + \bar{n}\,\mathrm{e}^{\mathrm{i}\omega t}]\} \tag{8}$$

where $S(T) = S_0(2\bar{n}+1)$, $S_0 = V^2/\omega^2$ is the Huang–Rhys factor and $\bar{n}$ is the phonon occupation number.

If at $t = 0$ a photon is absorbed, the function $I(t)$ describes the evolution of the absorption process. For $t \to \infty$ one can think that the vibrational quanta created by the absorption of the radiation have been destroyed through radiative and non-radiative decay and thus the limit of $I(t)$ for $t \to \infty$ provides the intensity of the zero-phonon (purely electronic) transition Ω_{if}. In the low-temperature limit ($\bar{n} \simeq 0$) the Fourier transform of equation (8) becomes:

$$I(\Omega) = |M_{\mathrm{odd}}|^2 \frac{1}{2\pi} \exp(-S_0) \int_{-\infty}^{+\infty} \exp[\mathrm{i}(\Omega - \Omega_{if})t] \exp\{S_0\,\mathrm{e}^{-\mathrm{i}\omega t}\} \exp(-\mathrm{i}\gamma|t|)\,\mathrm{d}t \tag{9}$$

where the inverse lifetime of the final vibronic state has been introduced as a damping factor γ. In the case of weak coupling (small S_0), by expanding the oscillating factor in equation (9), one finally gets the optical response function:

$$I(\Omega) = |M_{\mathrm{odd}}|^2\,\mathrm{e}^{-S_0} \sum_{n=0}^{\infty} \frac{S_0^n}{n!} \frac{\gamma}{\gamma^2 + (\Omega - \Omega_{if} - n\omega)^2}. \tag{10}$$

We see that equation (10) describes a sum of individual vibronic transitions of lorentzian lineshape, with natural halfwidth γ, centred at $\Omega = \Omega_{if} + n\omega$, whose intensities are affected by the factor $\mathrm{e}^{-S_0}\,S_0^n/n!$. It follows from the foregoing discussion that the δ-like Lorentz lines can be detected only when S_0 is small ($S_0 \ll 1$) and the temperature is very low. In the case of TMH the 'zero-phonon' line is then reinterpreted as the even zero-phonon line and the observed absorption band is due to the superposition of even-phonon progressions starting at different origins.

4. Discussion

The crystal-field absorption spectra of layered Mn halides have been studied by many authors (Pappalardo 1959, 1960, van Erk and Haas 1975, Pollini *et al* 1980). Different mechanisms, namely vibronic coupling with odd-parity vibrational modes, spin–orbit and exchange interactions between pairs of ions (Lohr and McClure 1968), have been proposed to explain the intensity of the parity- and spin-forbidden d–d transitions from the ground sextet ${}^6\mathrm{A}_{1\mathrm{g}}(\mathrm{e}^2\mathrm{t}_2^3)$ to the excited quartets of Mn^{2+} ions. The complicated fine structure of these absorption bands is, nevertheless, still far from receiving a complete assessment. In this paper we have reanalysed the multiphonon sidebands associated to the phonon-assisted transitions ${}^4\mathrm{A}_{1\mathrm{g}}(\mathrm{G})$, ${}^4\mathrm{E}_\mathrm{g}(\mathrm{G})$, and ${}^4\mathrm{E}_\mathrm{g}(\mathrm{D})$ of MnX_2 (X = Cl, Br, I) by means of a least-squares fitting based on equation (10) derived in § 3 in order to clarify whether the complex features occurring in such IC transitions can be interpreted in terms of first- and second-order progressions according to the selection rules worked out by Benedek *et al* (1979). We have taken as adjustable parameters the Huang–Rhys factors, the phenomenological damping factors and the oscillator strength for each phonon progression, while we have used the experimental values in order to fix the origins of the phonon progressions and to select the phonon energies involved in the absorption profile. Such calculations give results which are in good agreement with the attributions recently proposed by Pollini *et al* (1980), on the basis of the ligand field diagrams reported in the literature (König and Kremer 1977), except for the electronic transitions from the ground-state sextet to the excited quarters $^4E_g(D)$ in $MnCl_2$ and $^4A_{1g}(G)$ and $^4E_g(G)$ in MnI_2. Thus, in the following we will discuss in detail the last two vibronic transitions and attempt a more definite interpretation of the experimental data:

4.1. $MnCl_2$: $^4E_g(D)$

The strong IC character of $^4E_g(D)$ state is only weakly perturbed by spin–orbit mixing at the crossing with the $^4T_{1g}(P, e^3t_2^2)$ level. Thus it exhibits an A_{1g} progression, which is characterised by a weak e–p interaction, namely by a rapid intensity decrease with increasing phonon order. The weaker intercalated progression observed cannot however be assigned to a A_{1g} mode, the spacing being considerably larger. Since the theory also predicts no spin-dependent e–p interaction for this transition, the second progression is interpreted as due to a second-order $E_g \times E_g$ mode. As a matter of fact the least-squares fitting calculations reveal that three different progressions are necessary to describe all the important features of the spectrum. The result is shown in figure 2. The calculated phonon progressions with frequency spacing $\omega_1(E_g) = 130$, $\omega_2(A_{1g}) = 228$ and $\omega_3(E_g \times E_g) = 266\,\text{cm}^{-1}$ start at $\Omega_1 = 28100$, $\Omega_2 = 28092$ and $\Omega_3 = 28190\,\text{cm}^{-1}$ with Huang–Rhys factors given by $S_1 = 0.54$, $S_2 = 0.84$ and $S_3 = 1.02$ respectively. It should be noted that the best fitting is obtained using A_{1g} and E_g phonon frequencies which are slightly smaller than those observed in the Raman spectra (see figure 1). This can be interpreted in terms of the different relaxation of the excited states.

4.2. MnI_2: $^4E_g(G)$, $^4A_{1g}(G)$

Also the transitions to the quasi-degenerate levels $^4E_g(G)$, $^4A_{1g}(G)$ of MnI_2 are of IC character. Their degeneracy predicted in cubic approximation is removed by the trigonal field and thus we expect that the complicated phonon structures will not be explained in

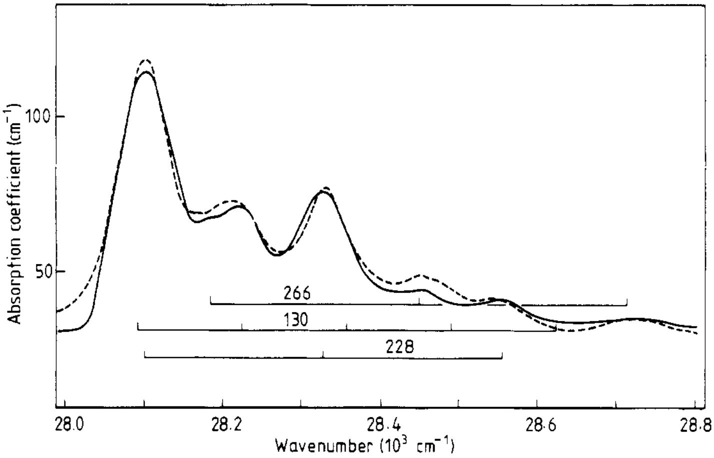

Figure 2. The crystal-field absorption due to the $^6A_{1g}(^6S) \rightarrow {}^4E_g(^4D)$ transition observed in $MnCl_2$ at 5 K (full curve) is compared with the theoretical profile (broken curve) calculated by means of equation (10).

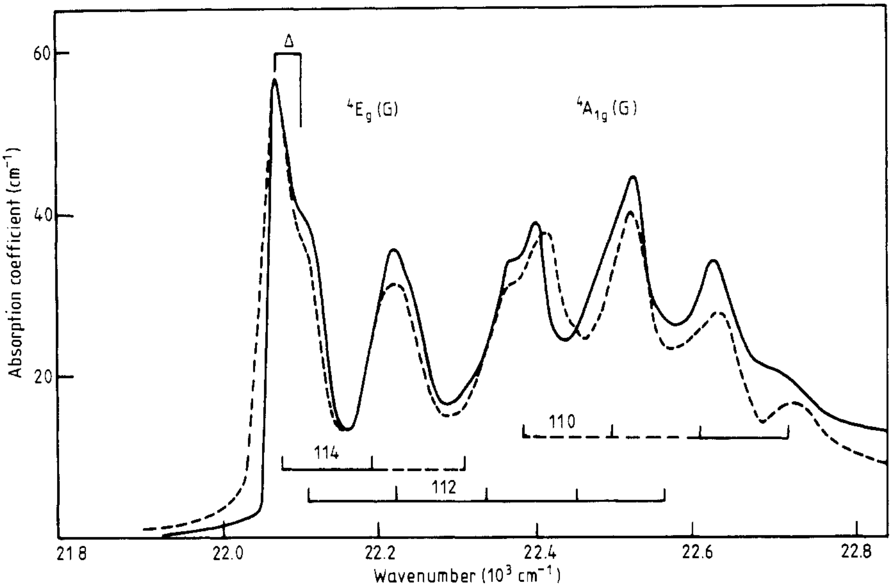

Figure 3. Crystal-field transition in MnI_2 due to the $^6A_{1g}(^6S) \rightarrow {}^4E_g(^4G), {}^4A_{1g}(^4G)$ transitions (full curve), taken from van Erk and Haas (1975). The broken curve refers to our calculated profile.

terms of a single vibronic progression. In fact, the peaks in the absorption spectrum have been previously assigned (van Erk and Haas 1975) to three progressions of A_{1g} modes with origins at 22062, 22105 and 22373 cm^{-1}. The origins at 22062 and 22105 cm^{-1} were assigned to the ^4E_g state and that at 22373 cm^{-1} to the $^4A_{1g}$ state. We have fitted the absorption curves by means of relation (10) in order to check whether the IC nature of the level would cause the superposition of two phonon series. The results reported in figure 3 show the comparison of the experimental curve and the computed profile obtained with three vibronic progressions with frequency distance $\omega_1(A_{1g}) = 114\ cm^{-1}$, $\omega_2(A_{1g}) = 112\ cm^{-1}$ and $\omega_3(A_{1g}) = 110\ cm^{-1}$. The calculated phonon progressions start at $\Omega_1 = 22072$, $\Omega_2 = 22107$, $\Omega_3 = 22373\ cm^{-1}$ with Huang–Rhys factors given by $S_1 = 0.28$, $S_2 = 1.34$ and $S_3 = 1.29$ respectively. The different origins of the progressions at Ω_1 and Ω_3 can be due to the $^4A_{1g}$–^4E_g separation of $\simeq 301\ cm^{-1}$ which was recently attributed to covalency (Hoekstra *et al* 1983). These authors have, moreover, assigned the sharp origin of the composite band starting around Ω_1, whose characteristic feature is a broad and asymmetric shape (width $\approx 80\ cm^{-1}$), to the zero-phonon magnetic dipole transition ^4E_g and the shoulder at Ω_2 to the exchange-induced transition $^4E_g + m$, where m is the energy of a magnetic excitation. This interpretation was based on low-temperature magnetic circular dichroism measurements and on the temperature dependence of the oscillator strength of the ^4E_g and ^4A_g bands. In this assumption the unusual linewidth has been attributed to the exciton dispersion and the peculiar lineshape has been correlated to the exciton density of states.

On the basis of our calculations we would however suggest an alternative interpretation. The lineshape of the band ^4E_g may be determined by considering Ω_1 and Ω_2 as starting points of two lorentzian progressions with linewidths $\gamma_1 = 9.35$ and $\gamma_2 = 26.17\ cm^{-1}$ respectively, which contribute to the formation of the optical profile. As we have suggested in a previous communication, we think that the origin of these first two progressions, shifted by $\Delta = 35\,\mathrm{cm}^{-1}$, would correspond to the frequency difference between the odd-parity transverse optical modes $\omega(A_{2u}) - \omega(E_u) = 37\,\mathrm{cm}^{-1}$ as measured in FIR transmission spectra (Paltrinieri *et al* 1982). This point of view is also supported by the fact that the strong intensity of the doubly forbidden band ^4E_g (Ω_1 origin) and its large bandwidth (see figure 3) are much larger than those corresponding to a magnetic dipole zero-phonon line ($\gamma \simeq 1$–$2\,\mathrm{cm}^{-1}$). Furthermore, in MnI_2 the vibronic coupling with odd-symmetry vibrations of T_{1u} type should be very strong, since these normal modes modulate directly the metal–ligand distance (Manson 1971). The trigonal distortion changes O_h symmetry into D_{3d} and lifts the phonon state degeneracy according to $T_{1u} \rightarrow E_u + A_{2u}$. Thus, in analogy to the case of $NiCl_2$ and $NiBr_2$ (Benedek *et al* 1979) this result can be interpreted in terms of a single forbidden electronic transition (^4E_g) assisted by two polar phonons of A_{2u} and E_u symmetry.

5. Conclusions

We have shown that for weak electron–phonon interaction and within the adiabatic and Condon approximations it is possible to derive a simple analytical expression for the absorption coefficient of TMH crystals. By using this expression in a least-squares fitting to the experimental bandshapes we have analysed the vibronic progressions of the parity- and spin-forbidden crystal-field bands $^4E_g(D)$, $^4E_g(G)$ and $^4A_{1g}(G)$ in Mn halides. We have found that, in general, the complex absorption profile is accurately reproducible by interpreting these progressions in terms of replicas of the Raman-active A_{1g} and E_g modes confirming most of the previous attributions. In some cases, however, the assignments supported by our calculations can improve those reported in the literature. The IC $^4E(D)$ transition in $MnCl_2$, for example, shows features that can be interpreted only if a two-phonon progression $E_g \times E_g$ is considered in addition to the two one-phonon progressions with spacing corresponding to the A_{1g} and E_g modes. This indicates that the attributions of the phonon progressions by simple inspection is sometimes misleading: in fact, it is difficult to take into account the role played by the Huang–Rhys factor, the phenomenological linewidth and the oscillator strength on the overall intensity distribution of the absorption band. In our opinion caution should also be taken before introducing additional mechanisms to explain the complicated structures observed in crystal-field transitions. It is possible, in fact, to explain the $^4E_g(G)$ transition in MnI_2 in terms of many-phonon processes induced by electron–phonon coupling, interpreting the broad and asymmetric peak around $22072\,\mathrm{cm}^{-1}$ as the ^4E_g transition assisted by two polar phonons.

Acknowledgments

The authors thank L Paltrinieri for his cooperation in recording the Raman and infrared spectra and G Benedek for useful discussions.

References

Benedek G and Frey G 1980 *Phys. Rev.* B **21** 2482
Benedek G, Pollini I, Piseri L and Tubino R 1979 *Phys. Rev.* B **20** 4303
Campbell J A and Vickers R E M 1983 *J. Phys. C: Solid State Phys.* **16** 999

Chiarotti G 1971 *Spectroscopy of Localised States, Trieste Lectures* (Vienna: IAEA) p 313

Christie J H 1973 *PhD Thesis* University of Canterbury, New Zealand

van Erk W and Haas C 1975 *Phys. Status Solidi* (b) **70** 517

Escribe C, Bouillot J and Ziebeck K R A 1980 *J. Phys. C: Solid State Phys.* **13** 4053

Hoekstra H J W M, Boudewijn P R, Groenier H and Haas C 1983 *Physica* **121**B 62

Knox R S 1973 *Solid State Phys.* Suppl. 5 (New York: Academic Press)

König E and Kremer S 1977 *Ligand Field Energy Diagrams* (New York: Plenum)

Kuindersma S R 1981 *Phys. Status Solidi* (b) **107** K163

Lohr L L and McClure D S 1968 *J. Chem. Phys.* **49** 3516

Manson N B 1971 *Phys. Rev.* B **4** 2656

McClure D S 1959 *Solid State Phys.* **9** 399 (New York: Academic Press)

Paltrinieri L, Piseri L and Pollini I 1982 *Proc. Int. Conf. on Raman Spectroscopy* (New York: Wiley) p 479

Pappalardo P 1959 *J. Chem. Phys.* **31** 1050

—— 1960 *J. Chem. Phys.* **33** 613

Perlin Yu E 1964 *Sov. Phys.–Usp.* **6** 542

Pollini I, Spinolo G and Benedek G 1980 *Phys. Rev.* B **22** 6369

Sugano S, Tanabe Y and Kamimura H 1970 *Multiplets of Transition–Metal Ions in Crystals* (New York: Academic Press)

Sumi H 1974 *J. Phys. Soc. Japan* **36** 770

—— 1975 *J. Phys. Soc. Japan* **38** 825

Wyckoff R W G 1972 *Crystal Structures* vol 1 (New York: Interscience)

Yelon W B, Vettier C, Pasternak A and Guggenheim H 1980 *J. Phys. C: Solid State Phys.* **13** 5863